Phonon density of states of Fe_{2}O_{3} across high-pressure structural and electronic transitions

Jung-Fu Lin, John S. Tse, Esen E. Alp, Jiyong Zhao, Michael Lerche, Wolfgang Sturhahn, Yuming Xiao, and Paul Chow

Phys. Rev. B **84**, 064424 — Published 24 August 2011

DOI: 10.1103/PhysRevB.84.064424

Phonon Density of States of Fe_2O_3 across High-Pressure Structural and Electronic Transitions

Jung-Fu Lin[1], John S. Tse[2], Esen E. Alp[3], Jiyong Zhao[3], Michael Lerche[4], Wolfgang Sturhahn[3], Yuming Xiao[5], Paul Chow[5]

[1]*Department of Geological Sciences, Jackson School of Geosciences, The University of Texas at Austin, TX 78712, USA*
[2]*Department of Physics and Engineering Physics, University of Saskatchewan, Saskatoon, SK S7N 5E2, Canada*
[3]*Advanced Photon Source, Argonne National Laboratory, Argonne, IL 60439, USA*
[4]*McClellan Nuclear Research Center, University of California, Davis, McClellan, CA 95652, USA*
[5]*HPCAT, Carnegie Institution of Washington, Advanced Photon Source, Argonne National Laboratory, Argonne, IL 60439, USA*

Abstract

High-pressure phonon density of states of Fe_2O_3 across structural and electronic transitions has been investigated by nuclear resonant inelastic X-ray scattering and first-principles calculations, together with synchrotron Mössbauer, X-ray diffraction, and X-ray emission spectroscopies. Drastic changes in elastic, thermodynamic, and vibrational properties of Fe_2O_3 occur across the Rh_2O_3(II)-type structural transition at 40-50 GPa, whereas the Mott insulator-metal transition occurring after the structural transition only causes nominal changes in the properties of the Fe_2O_3. The observed anomalous mode softening behavior of the elastic constants is associated with the structural transition at 40-50 GPa, leading to substantial changes in the Debye-like part of the PDOS in the terahertz acoustic phonons. Our experimental and theoretical studies provide new insights into the effects of the structural and electronic transitions in the transition metal oxide compounds.

Introduction

Hematite (Fe_2O_3), an antiferromagnetic insulator under ambient conditions, is regarded as an archetypal Mott-insulator for the trivalent transition-metal oxides (TMOs), the majority of which crystallize in the corundum-type structure [1,2]. Since iron is the most abundant transition metal in the Earth, hematite as an end-member ferric iron (Fe^{3+}) oxide is also an important proxy for characterizing the oxidation state, geomagnetism, and geochemistry of the planet's interior [3-5]. Recent multidisciplinary studies have shown that hematite undergoes a number of transitions under high pressures including structural, insulator-metal, magnetic collapse, and electronic spin-pairing transitions [5-18]. Of particular interest is the pressure-induced Mott insulator-metal transition with the breakdown of the strong electronic *d-d* correlation and closure of the Mott-Hubbard *d-d* band gap, resulting in a metallic phase with zero moment at approximately 50 GPa [1,10-12,18]. Although the Mott transition was first proposed to occur concurrently with the Rh_2O_3(II)-type structural and electronic transition, effectively decreasing the Fe^{3+} radius and the unit cell volume in the shift to the low-spin paramagnetic state, the metallic state is reported to occur in the Rh_2O_3(II)-type phase [5-18]. This observation calls for further understanding on the interplays and associated effects between the structural, electronic, and magnetic transitions in Fe_2O_3 at high pressures.

Electronic and structural transitions in the TMOs have been recently found to significantly affect their physical and chemical properties under high pressures [19-25]. Specifically, the electronic spin-pairing transition of iron in ferropericlase ((Mg,Fe)O), an abundant mineral in the Earth's lower mantle, is found to result in changes in density, some of the elastic constants, and transport and rheological properties, which in turn affect a broad spectrum of geophysical, geochemical, and geodynamic implications of the

deep Earth [22-24]. Furthermore, recent studies in the TMOs under high pressures also show anomalous softening in elasticity as a result of the strong phonon-magnon coupling, leading to substantial changes in the Debye-like part of the phonon density of states (PDOS) [19-20]. Understanding the high-pressure PDOS behavior of hematite is particularly interesting because of the multiple aforementioned transitions and their potential couplings. Yet, the effects of these transitions on elastic, thermodynamic, and vibrational properties of Fe_2O_3 remain largely lacking. Here we have measured the partial PDOS of iron in Fe_2O_3 by nuclear resonant inelastic X-ray scattering (NRIXS) up to 85 GPa in a diamond anvil cell (DAC). NRIXS is a relatively new synchrotron technique that has been successfully applied to study lattice dynamics of ^{57}Fe-containing compounds under extreme pressures and temperatures [25-28]. Together with first-principles theoretical calculations, the PDOS are used to characterize the behavior of Fe_2O_3 across the structural and electronic transitions. We observed significant softening in the elastic properties as well as other major changes in thermodynamic and vibrational properties of Fe_2O_3 between 40 and 50 GPa, which are attributed to the structural transition in hematite. The magnetic collapse is reported to occur in the Rh_2O_3(II) phase between 55 GPa and 75 GPa, causing only nominal changes in the PDOS of the Fe_2O_3.

Experimental Details

^{57}Fe-enriched Fe_2O_3 (>95% enrichment) was purchased from the Cambridge Isotope Laboratories, Inc., and was characterized for its crystal structure and chemical composition by X-ray diffraction and electron microprobe analyses, respectively. Samples measuring approximately 25 μm thick and 40 μm wide were loaded into DACs with 300 μm flat culets or beveled diamonds (150 μm in the inner culets and 300 μm in

the outer culets) with Be gaskets of 3 mm in diameter and cubic BN gasket inserts. Pressures were determined from the ruby spheres in the sample chamber using the ruby fluorescence scale [29]. High-pressure NRIXS experiments were conducted at sector 3 of the Advanced Photon Source (APS), Argonne National Laboratory (ANL) [25-28]. Energy spectra were obtained by tuning the X-ray energy (approximately $\pm$80 to $\pm$95 meV in steps of 0.25 meV) around the nuclear transition energy of 14.4125 keV with an energy resolution of 1 meV and an X-ray beamsize of approximately 10 μm. The Kα,β fluorescence radiation from the ^{57}Fe-enriched Fe_2O_3 sample, emitted with time delay relative to the incident X-ray pulses due to the lattice excitations of the iron sublattice, was collected by three avalanche photodiode detectors (APD), whereas the synchrotron Mössbauer spectroscopy (SMS) spectra were collected by a fourth detector in the forward direction. A quasi-harmonic model was used to extract the PDOS from the measured energy spectra (Fig. 1) [25-27]. In this model, the atomic motions relative to the temperature-dependent averaged position are assumed to be harmonic under the given conditions of pressure, temperature, and other parameters. Thermal effects such as change of force constants with atomic distances are allowed to change, but the vibrations are still assumed to occur in a harmonic potential [25-27]. Previous studies have confirmed the reliability of this model to extract the PDOS and the bulk Debye sound velocity (V_D) of Fe-containing compounds under high pressures [28].

Experimental Results

Elastic, thermodynamic and vibrational properties of the iron component in Fe_2O_3 have been derived from the integration of the measured PDOS in Fe_2O_3 (Figs. 1,2). The V_D of the sample is derived from parabolic fitting of the low-energy slope of the PDOS in

the range of approximately 0.2 meV to 15 meV (Fig. 2) [26,27]. In this lattice dynamics model, the Debye velocity of a material is derived from the initial slope of the density of states versus energy squared (E^2) plot (a parabolic function in the PDOS versus energy). In the acoustic region, the translation motions of all the atoms in the system (in this case both Fe and O) are in phase. Therefore, the Debye velocity estimated from the Fe PDOS should be exactly the same as from the full consideration of the density of states. The Debye theory is valid for the acoustic modes in the harmonic solids with Debye-like low-frequency dynamics, and Fe_2O_3 has been shown to exhibit Debye-like lattice dynamic behavior in previous studies [28]. It has also been demonstrated that the Debye sound velocity (V_D) measured in NRIXS corresponds to the V_D of the whole matrix (not the Fe atoms alone) [28]. That is, the projected density of states of Fe represents the total phonon density of states of Fe_2O_3 in the low-frequency region. For this reason, the extraction of the long wavelength properties of the Fe_2O_3 from just the Fe partial DOS is thus in principle valid.

The characteristic temperature or Lamb-Mössbauer temperature (T_{LM}) in Fig. 2 is defined as:

$$\frac{1}{T_{LM}} = k_B \int \frac{2E_{\mathrm{Re}coil}}{E^2} g(E) dE$$

where k_B is the Boltzmann's contant, E_{recoil} is the recoil energy for ^{57}Fe nucleus (1.96 meV), and g(E) is the partial phonon density of states. The recoil free fraction, commonly known as Lamb-Mössbauer factor (f_{LM}), is related to the characteristic temperature, or Lamb-Mössbauer temperature (T_{LM}), as follows:

$$-\ln f_{LM}(T) = \frac{T}{T_{LM}} = k_0^2 \langle x^2 \rangle$$

where k_0 is the momentum of the photons with 14.412 keV, which equals to 7.3 Å, and $\langle x^2 \rangle$ is the average displacement. One can also relate T_{LM} to the Debye temperature, as follows:

$$-\ln f_{LM}(T) = k_B T \frac{6E_{Recoil}}{E_D^2(T)}$$

where E_D is the Debye cut-off energy, as given by the maximum in the Debye distribution of the phonon density of states. Hence, $T_{LM} = \frac{E_D^2}{6k_B E_{Recoil}}$.

Abnormal behavior of these properties is observed to occur between 40 GPa and 50 GPa. Specifically, V_D, the mean force constant (D_{av}), and the Lamb-Mössbauer factor (f_{LM}) suddenly drop between 40 and 50 GPa, suggesting a softening in Fe_2O_3 in this pressure range. Furthermore, vibrational specific heat (C_{vib}) and vibrational entropy (S_{vib}) decrease with increasing pressures, but jump significantly between 40 and 50 GPa. To understand these observations, we have employed X-ray diffraction, SMS, and X-ray emission spectroscopy (XES) to confirm the crystal structures, hyperfine parameters, and total spin momentum of Fe_2O_3 under high pressures, respectively (Fig. 3,4). X-ray diffraction spectra were consistent with a structural transition from the corundum to the Rh_2O_3(II) structure that has been reported to occur at approximately 40-50 GPa [7-10], whereas the SMS and XES results indicated that the magnetic collapse occurs in the high-pressure Rh_2O_3(II) phase and is completed at approximately 75 GPa, consistent with previous studies [5-15,18] (Fig. 3,4).

Theoretical Calculations

In order to qualitatively decipher the interplay between the structural, magnetic, and electronic transitions of Fe_2O_3 under high pressures, first-principles electronic and

147 phonon calculations using the VASP suite program were performed to investigate
148 structural and magnetic transitions in hematite (Fig. 5-8) [30-33]. Projected augmented
149 (PAW) potentials were used for both the Fe and O atoms, and the semi-core 3*s* and 3*p*
150 orbitals of Fe were treated as valence [31,32]. The rotationally-invariant LSDA+U model
151 with the Perdew-Burke-Ernzerhof (PBE) exchange correlation function (U=4.0 eV and J
152 = 0.9 eV) in the Generalized Gradient Approximation (GGA) was used to model the
153 strongly correlated Fe 3*d* states in the AFM corundum structure [30-32]. Based on
154 previous studies [14], we have used the Rh_2O_3(II)-type structure (space group: *Pbcn*)
155 with experimentally-reported lattice parameters for our theoretical calculations for the
156 high-pressure phase [14]. It is well known that it is necessary to include the Hubbard U to
157 describe the band gap of the insulating magnetic state. Whether it is necessary to involve
158 the Hubbard U term to describe the metallic non-magnetic state is not certain. We have
159 performed calculations with the same Hubbard U parameter as in the corundum structure
160 but the calculated PDOS does not agree with experimental results at all. The GGA
161 method, on the other hand, agrees well with experiments, leading us to rule out the use of
162 the Hubbard U in the calculations. It is found that the GGA approximation is consistent
163 with experimental results and adequate to describe the electron and phonon structures of
164 the high pressure non-magnetic Rh_2O_3 (II) phase (Fig. 5) [34]. Phonon dispersion and Fe
165 projected density of states (PDOS) were calculated with the small displacement method
166 [33] employing supercells constructed from a 2×2×2 replicate of the corundum structure
167 and a 1×2×2 replicate of the Rh_2O_3(II) crystallographic unit cell. Calculations were
168 performed at 40 GPa for the AFM corundum-type phase, at 55 GPa for both the non-
169 magnetic (NM) corundum-type phase and AFM Rh_2O_3(II)-type phase, and at 70 GPa for
170 the NM Rh_2O_3(II) (Figs. 5-8). We have also calculated the stability of the NM corundum

and AFM Rh_2O_3(II) structures at these pressures and have found them to be unstable when compared to the AFM corundum and NM Rh_2O_3(II) structures.

The theoretical Fe PDOS of the AFM corundum structure at 40 GPa and the NM Rh_2O_3 (II) structure at 70 GPa are compared with corresponding experimental results in Fig. 5a and 5c, respectively. The experimentally observed decrease in V_D of 14% from the magnetic corundum to metallic Rh_2O_3(II) phase is correctly reproduced by the calculated value of 16% (Figs. 2,5). The agreements are very good and all the salient features of the experimental PDOS are correctly reproduced. The most distinctive differences in the calculated vibrational PDOS features are the drastic shift of the first PDOS peak from approximately 21 meV in the AFM corundum-type phase to approximately 37 meV in the AFM Rh_2O_3(II)-type structure at 55 GPa, and as a consequence, a significant drop in the gradient of the acoustic phonon dispersion. These predictions are qualitatively consistent with experimental observations on the softening of the Debye sound velocity across the structural transition (Figs. 1,5). There are also shifts in the high frequency vibrations, dominated by the oxygen motions, to higher energy. Across the structural transition, the Debye sound velocity suddenly becomes much slower in the Rh_2O_3(II)-type phase than in the corundum-type phase; though, it should be noted that these phases are all in the AFM state. In absence of the structural transition, the low-frequency Debye-like vibrations in the corundum-type and the Rh_2O_3(II)-type structures, respectively, behave rather normally with a weak pressure effect; this weak pressure effect persists across the AFM to the NM transition in the Rh_2O_3(II)-type phase, suggesting that electronic transitions do not significantly affect elastic and vibrational properties of Fe_2O_3 at high pressures.

Discussion

Based on our experimental results and first-principles calculations, here we address how the properties of Fe_2O_3 are affected by structural and electronic transitions under high pressures. Together with the previous studies, it is now well documented that the transition from the AFM hematite to the AFM Rh_2O_3(II) phase occurs at approximately 40-50 GPa with a volume reduction of approximately 10% and the shortening of the bond lengths [5-15]. Our observed dramatic changes in the elastic, vibrational, and thermodynamic properties correspond to the structural transition to the AFM Rh_2O_3(II)-type occurring at 40-50 GPa, without the involvement of the spin-pairing and magnetic collapse transitions. This structural transition is thus associated with the softening in the lattice vibrational phonons in Fe_2O_3 and significant reductions in the V_D, Lamb-Mössbauer factor, and the mean force constant, among others. The drop in the V_D across the transition suggests that compressional and shear velocities of Fe_2O_3 would also decrease significantly as well. On the other hand, the mean force constant represents the short-range repulsive, interatomic forces arising from the charge distributions and Hund's rules of atoms, and its decrease thus corresponds to a softening in the lattice incompressibility and likely the lattice strength within the transition. The Lamb-Mössbauer factor is related to the mean-square displacement of the iron atoms in the lattice, $\langle x^2 \rangle$, through $f_{LM}=\exp(-k^2\langle x^2 \rangle)$, where k is the wave number of the resonant X-ray. That is, the structural transition reduces the lattice displacement of the Fe^{3+} atoms and is manifested in the reduction of the Lamb-Mössbauer factor by approximately 5%. This transition also results in an increase in the thermodynamic vibrational heat capacity and entropy.

Previous studies showed that the electronic transition and the magnetic collapse, the Mott transition, occur at higher pressures only in the Rh_2O_3(II) phase [13]. A Mott transition, as defined by Mott himself, is an isostructural paramagnetic metal to paramagnetic insulator transition [1,21]. This isostructural transition implies that the crystal symmetry of the Rh_2O_3(II) phase is preserved across the magnetic collapse. Our studies, together with previous results [7-14], confirm this behavior, in which the AFM character with magnetic moments persists up to approximately 75 GPa before the magnetic collapse is fully completed. Based on our NRIXS results and first-principles calculations, the Mott transition does not significantly affect the elastic, thermodynamic, and vibrational properties of the Rh_2O_3(II)-type Fe_2O_3; these properties change rather monotonically with increasing pressures (Fig. 2). The high-spin AFM Rh_2O_3(II)-type phase is found to be dynamically unstable at 55 GPa in our calculations, and a soft phonon mode is found at the M symmetry point.

Conclusions

In summary, significant changes in the PDOS of Fe_2O_3 were observed with the softening on the sound velocities, interatomic force constant, and Lamb-Mössbauer factor associated with the corundum-type to the Rh_2O_3(II)-type structural transition at 40-50 GPa, but the isostructural Mott transition only occurs in the Rh_2O_3(II) phase and does not have a strong effect on the properties of Fe_2O_3. The structural transition under pressure corresponds to anomalous mode softening behavior of the elastic constants preceding the Mott transition, leading to substantial changes in the Debye-like part of the PDOS in the terahertz acoustic phonons. Our studies on the high-pressure behavior of the archetypal

241 Fe_2O_3 here provide new insights into the effects of the structural and electronic
242 transitions in the TMO compounds.

243 We acknowledge XOR-3 and GSECARS, APS, ANL for the use of the synchrotron
244 and laser facilities, and TACC for the computational facilities. Use of the Advanced
245 Photon Source was supported by U.S. Department of Energy (DOE), Office of Science,
246 Basic Energy Sciences (BES), under contract No. DE-AC02-06CH11357. J.F.L.
247 acknowledges financial support from Energy Frontier Research in Extreme Environments
248 (EFree) Center, NSF Earth Sciences (EAR-0838221), and Carnegie/DOE Alliance Center
249 (CDAC).

250

251 [1] N. Mott, Metal-Insulator Transitions (Taylor & Francis, London, 1960).
252 [2] I.S. Lyubutin, S.G. Ovchinnikov, A.G. Gavriliuk, and V.V. Struzhkin, Phys. Rev. B
253 **79**, 085125 (2009).
254 [3] D.P. Dobson and J.P. Brodholt, Nature **434**, 371 (2005).
255 [4] C. McCammon, Science **308**, 807 (2005).
256 [5] E. Ito, H. Fukui, T. Katsura, D. Yamazaki, T. Yoshino, Y. Aizawa, A. Kubo, S.
257 Yokoshi, K. Kawabe, S. Zhai, A. Shatzkiy, M. Okube, A. Nozawa, and K.-I.
258 Funakoshi, Am. Mineral. **94**, pages 205 (2009).
259 [6] R.D. Shannon and C.T. Prewitt, J. Solid State Chem. **2,** 134 (1970).
260 [7] T. Yagi and S. Akimoto, in High Pressure Research in Geophysics, edited by S.
261 Akimoto and M. Manghnani (Kluwer Academic, Tokyo, 1982), p. 81.
262 [8] Y. Syono, A. Ito, S. Morimoto, S. Suzuki, T. Yagi, and S. Akimoto, Solid State
263 Commun. **50**, 97 (1984).
264 [9] E. Knittle, and R. Jeanloz, Solid State Commun. **58**, 129 (1986).

265 [10] J.S. Olsen, C. Cousins, L. Gerward, H. Jhans, and B. Sheldon, Phys. Scr. **43**, 327
266 (1991).
267 [11] M.P. Pasternak, G. Kh. Rozenberg, G.Yu. Machavariani, O. Naaman, R.D. Taylor,
268 and R. Jeanloz, Phys. Rev. Lett. **82**, 4663 (1999).
269 [12] J.-P. Rueff, C.-C. Kao, V. Struzhkin, J. Badro, J.-F. Shu, R. Hemley, and H.-K. Mao,
270 Phys. Rev. Lett. **82**, 3284 (1999).
271 [13] J. Badro, G. Fiquet, V.V. Struzhkin, M.S. Somayazulu, H.K. Mao, G. Shen, and T.
272 Le Bihan, Phys. Rev. Lett. **89**, 205504 (2002).
273 [14] G. Rozenberg, L. Dubrovinsky, M. Pasternak, O. Naaman, T.L. Bihan, and R.
274 Ahuja, Phys. Rev. B **65**, 064112 (2002).
275 [15] S. Ono, T. Kikegawa, and Y. Ohishi, J. Phys. Chem. Solids **65**, 1527 (2004).
276 [16] J. Kunes, D.M. Korotin, M.A. Korotin, V.I. Anisimov, and P. Werner, Phys. Rev.
277 Lett. **102**, 146402 (2009).
278 [17] N.C. Wilson, S.P. Russo, Phys. Rev. B **79**, 094113 (2009).
279 [18] S. Wang, W.L. Mao, A.P. Sorini, C.-C. Chen, T. P. Devereaux, Y. Ding, Y. Xiao, P.
280 Chow, N. Hiraoka, H. Ishii, Y.Q. Cai, and C-C. Kao, Phys. Rev. B **82**, 144428
281 (2010).
282 [19] V.V. Struzhkin, H.K. Mao, J. Hu, M. Schwoerer-Böhning, J. Shu, R.J. Hemley, W.
283 Sturhahn, M.Y. Hu, E.E. Alp, P. Eng, and G. Shen, Phys. Rev. Lett. **87**, 255501
284 (2001).
285 [20] A.P. Kantor, S.D. Jacobsen, I.Yu. Kantor, L.S. Dubrovinsky, C.A. McCammon, H.J.
286 Reichmann, and I.N. Goncharenko, Phys. Rev. Lett. **93**, 215502 (2004).

[21] C.S. Yoo, B. Maddox, J.-H.P. Klepeis, V. Iota, W. Evans, A. McMahan, M. Hu, P. Chow, M. Somayazulu, D. Hausermann, R.T. Scalettar, and W.E. Pickett, Phys. Rev. Lett. **94**, 115502 (2005).

[22] J.F. Lin, S.D. Jacobsen, W. Sturhahn, J.M. Jackson, J. Zhao, and C.S. Yoo, Geophys. Res. Lett. **33**, L22304 (2006).

[23] D. Antonangeli, J. Siebert, C.M. Aracne, D.L. Farber, A. Bosak, M. Hoesch, M. Krisch, F.J. Ryerson, G. Fiquet and J. Badro, Science **331**, 64 (2011).

[24] R.M. Wentzcovitch, J.F. Justo, Z. Wu, C.R.S. da Silva, D. Yuen, and D. Kohlstedt, Proc. Natl. Acad. Sci. USA **106**, 8447 (2009).

[25] W. Sturhahn and K.G. Kohn, Hyperfine Interact. **123/124**, 367 (1999).

[26] W. Sturhahn, Hyperfine Interact. **125**, 149 (2000).

[27] W. Sturhahn, J. Phys. Condens. Matter **16,** S497 (2004).

[28] M. Hu, W. Sturhahn, T.S. Toellner, P.D. Mannheim, D.E. Brown, J. Zhao, and E.E. Alp, Phys. Rev. B **67**, 094304 (2003).

[29] H.K. Mao, P.M. Bell, J.W. Shaner, and D.J. Steinberg, J. Appl. Phys. **49**, 3276 (1978).

[30] J.P. Perdew, K. Burke, and M. Ernzerhof, Phys. Rev. Lett. **77**, 3865 (1996).

[31] G. Kresse, and J. Furthmuller, Comp. Mater. Sci. **6**, 15 (1996).

[32] G. Kresse, and J. Furthmuller, Phys. Rev. B **54**, 11169 (1996).

[33] Z. Li, and T.S. Tse, Phys Rev B **61**, 1453 (2000).

[34] H. W. Sheng, H.W. Sheng, H.Z. Liu, Y.Q. Cheng, J. Wen, P.L. Lee, W.K. Luo, S.D. Shastri, and E. Ma, Nat. Mater. **6**, 192-196, 2007.

Figure Captions:

FIG 1. Representative PDOS of Fe from $^{57}Fe_2O_3$ at high pressures. The PDOS spectra are derived from the NRIXS experiments in a high-pressure diamond anvil cell. Experimental error bars are shown as vertical gray bars.

FIG 2. Elastic, thermodynamic, and vibrational parameters of Fe_2O_3 as a function of pressure obtained from integration of the PDOS. **(a)** Debye sound velocity; **(b)** mean force constant, D_{av}; **(c)** Lamb-Mössbauer factor, f_{LM}; **(d)** vibrational specific heat, C_{vib} (k_B, Boltzmann constant); **(e)** vibrational entropy, S_{vib}; **(f)** characteristic temperature or Lamb-Mössbauer temperature, T_{LM}. We note that these values only represent the contribution of the Fe sublattice in Fe_2O_3. Using the theoretical densities we computed the sound velocities of Fe_2O_3 in the corundum structure at 40 GPa and Rh_2O_3(II) structure at 70 GPa to be 4.7 km/s and 3.8 km/s, respectively.

FIG 3. (Color Online) Representative X-ray diffraction **(a)** and Fe-Kβ X-ray emission **(b)** patterns of Fe_2O_3 at high pressures. X-ray diffraction spectra confirmed the structural transition from the corundum-type to the Rh_2O_3(II)-type phase at high pressures. The intensity of the satellite K_{β}‘ peak can be used to understand the electronic spin-pairing and metallization in Fe_2O_3. Its intensity remains similar across the structural transition, but reduces significantly at higher pressures.

FIG 4. (Color Online) **(a)** Representative synchrotron Mössbauer spectra (SMS) of Fe_2O_3 at high pressures. Corresponding energy spectra calculated from the fits are shown in the right panels. Red dots: experimental SMS spectra; black lines: modeled spectra. **(b)**. Analyzed hyperfine parameters and percentage of the magnetic phase in high-pressure Fe_2O_3. Up to 55 GPa, the only spectral component is that of the low-pressure magnetic phase characterized by the hyperfine field of 51 T, a typical value of the hyperfine field

for ionic ferric oxide bonding. A nonmagnetic quadrupole-split component emerges at approximately 55 GPa, which we assigned as the high-pressure component, coexisting with the low-pressure magnetic-split component. The relative abundance of the low-pressure component continues to decrease until the magnetic collapse is completed at around 75 GPa. We note that the hyperfine field of the magnetic component is slightly reduced by about 10% within the transition.

FIG 5. (Color Online) Projected Fe vibrational phonon density of states (PDOS) of Fe_2O_3 at high pressure from first-principles calculations. **(a)** the AFM corundum-type phase at 40 GPa; **(b)** the theoretical AFM corundum-type phase (black line) and the NM Rh_2O_3(II)-type phase (red line) at 55 GPa; Black lines, corundum-type phase; red lines: Rh_2O_3(II)-type phase; **(c)** the NM Rh_2O_3(II)-type phase at 75 GPa. The black and red circles in (a) and (c) represent the experimental and theoretical Fe PDOS, respectively.

FIG 6. Calculated GGA phonon dispersive curves (top) and Fe projected density of states (bottom) of the non-magnetic Rh_2O_3 (II) structure of Fe_2O_3 at 55 GPa.

FIG 7. Calculated GGA phonon dispersive curves (top) and Fe projected density of states (bottom) of the non-magnetic Rh_2O_3 (II) structure of Fe_2O_3 at 70 GPa.

FIG 8. (Color Online) Calculated Fe projected density of states and total density of states of Fe_2O_3 in the corundum structure (top) and Rh_2O_3 (II) structure (bottom).

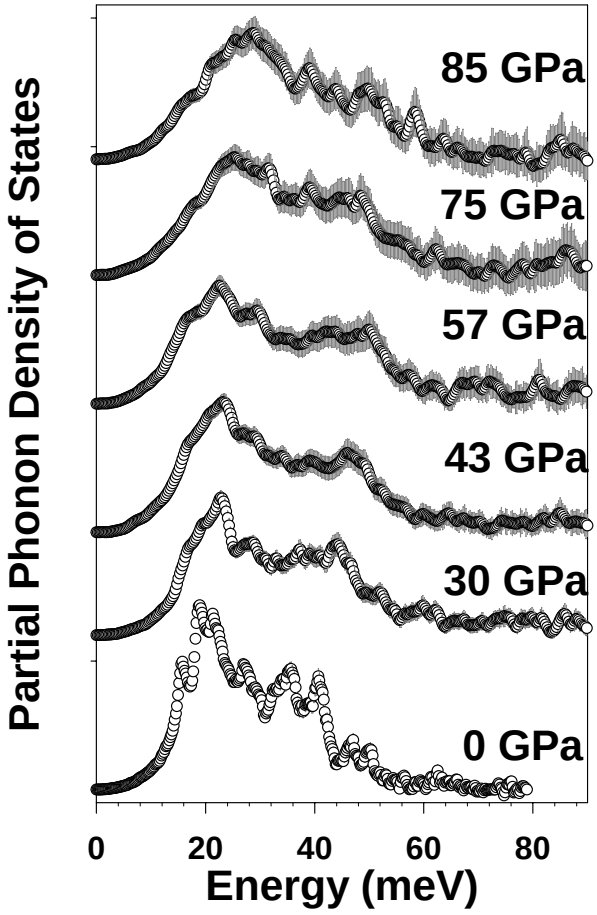
Partial Phonon Density of States
85 GPa
75 GPa
57 GPa
43 GPa
30 GPa
0 GPa
0
20
40
60
80
Energy (meV)

FIG. 1

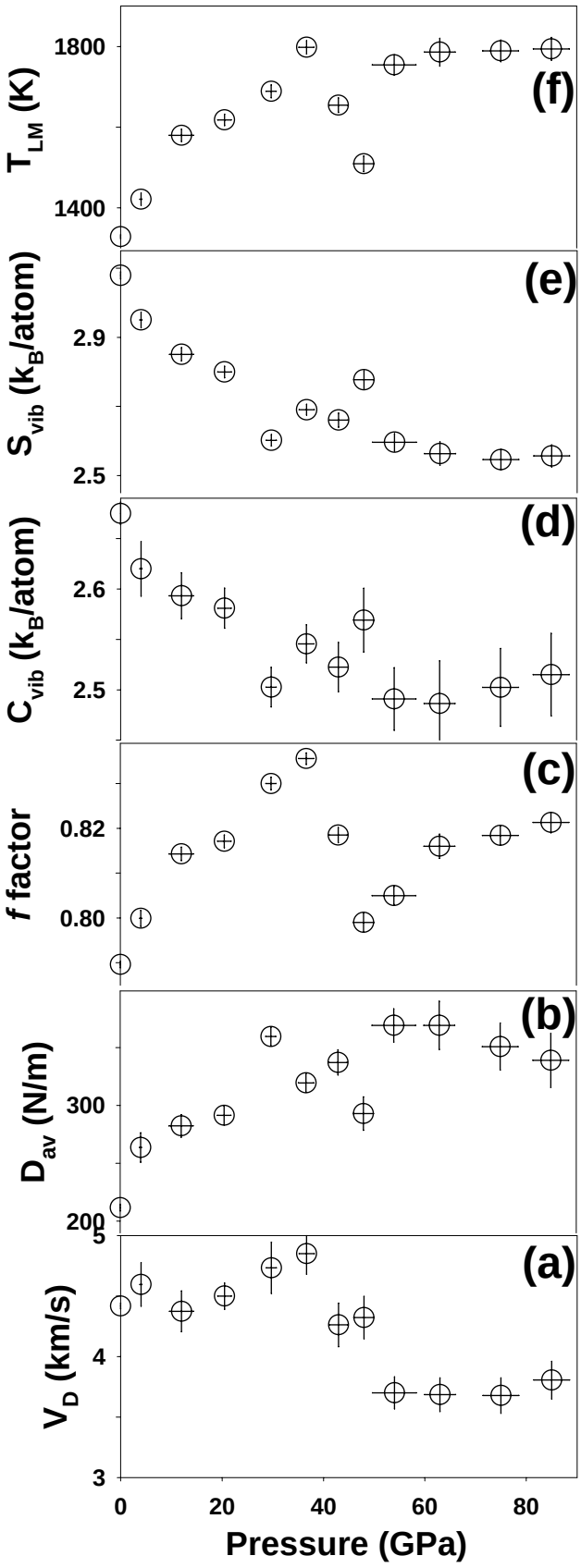
(f)
T_{LM} (K)
1800
1400
(e)
S_{vib} (k_B/atom)
2.9
2.5
(d)
C_{vib} (k_B/atom)
2.6
2.5
(c)
f factor
0.82
0.80
(b)
D_{av} (N/m)
300
200
(a)
V_D (km/s)
5
4
3
0
20
40
60
80
Pressure (GPa)

FIG. 2

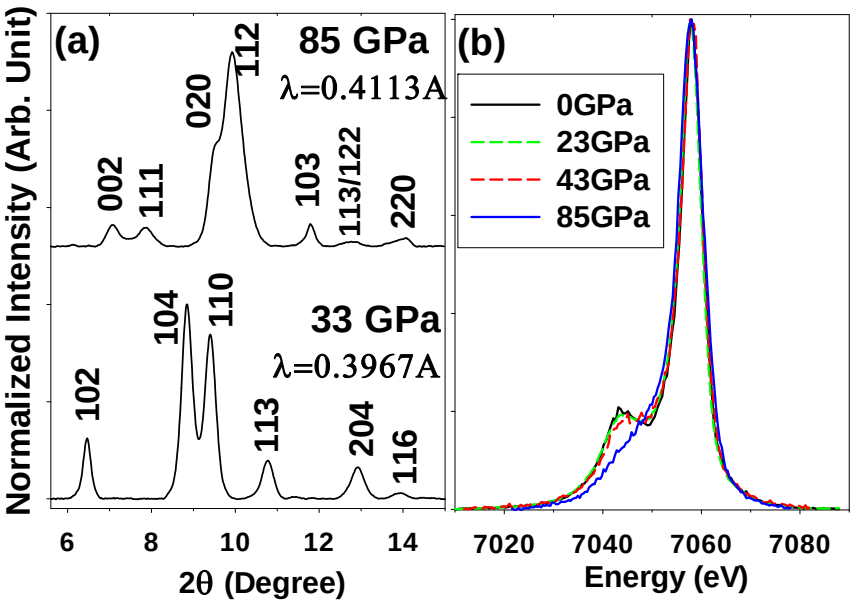
(a)
85 GPa
λ=0.4113A
002
111
020
112
103
113/122
220
33 GPa
λ=0.3967A
102
104
110
113
204
116
Normalized Intensity (Arb. Unit)
6
8
10
12
14
2θ (Degree)
(b)
0GPa
23GPa
43GPa
85GPa
7020
7040
7060
7080
Energy (eV)

FIG. 3

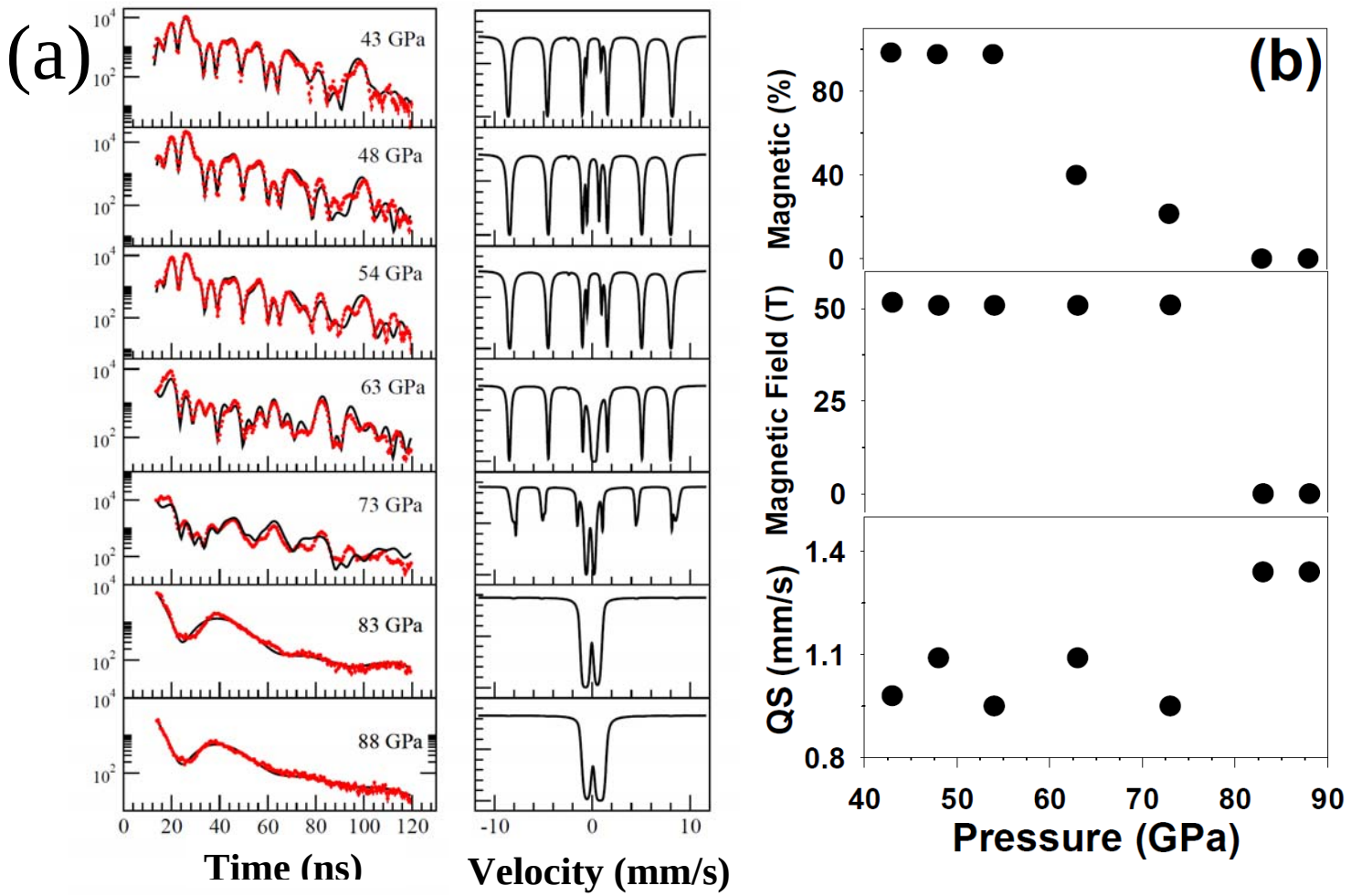
(a)
43 GPa
48 GPa
54 GPa
63 GPa
73 GPa
83 GPa
88 GPa
Time (ns)
Velocity (mm/s)
(b)
Magnetic (%)
Magnetic Field (T)
QS (mm/s)
Pressure (GPa)

FIG4

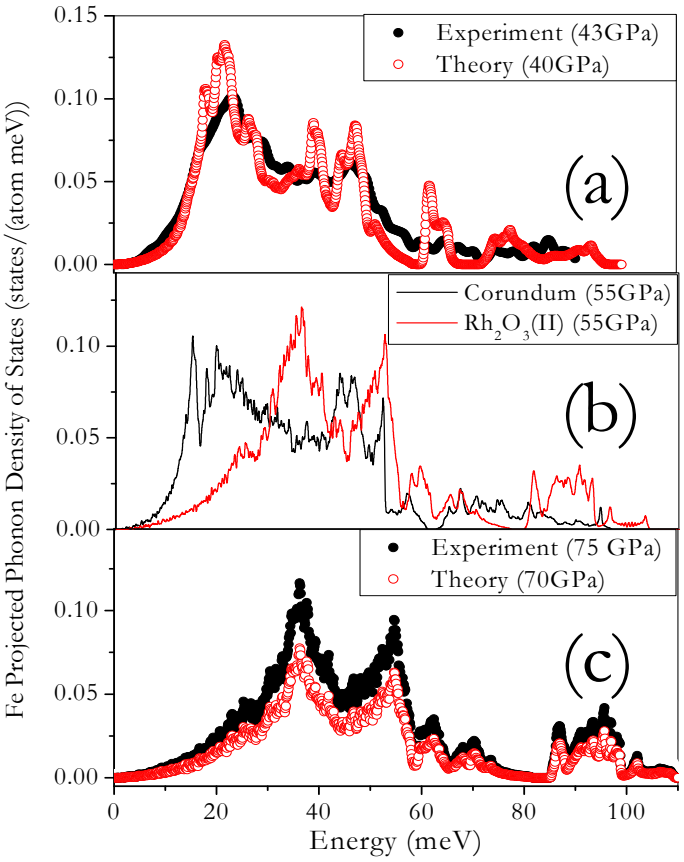
Experiment (43GPa)
Theory (40GPa)
(a)
Corundum (55GPa)
Rh2O3(II) (55GPa)
(b)
Experiment (75 GPa)
Theory (70GPa)
(c)
Fe Projected Phonon Density of States (states/(atom meV))
Energy (meV)
0.15
0.10
0.05
0.00
0
20
40
60
80
100

Fig. 5

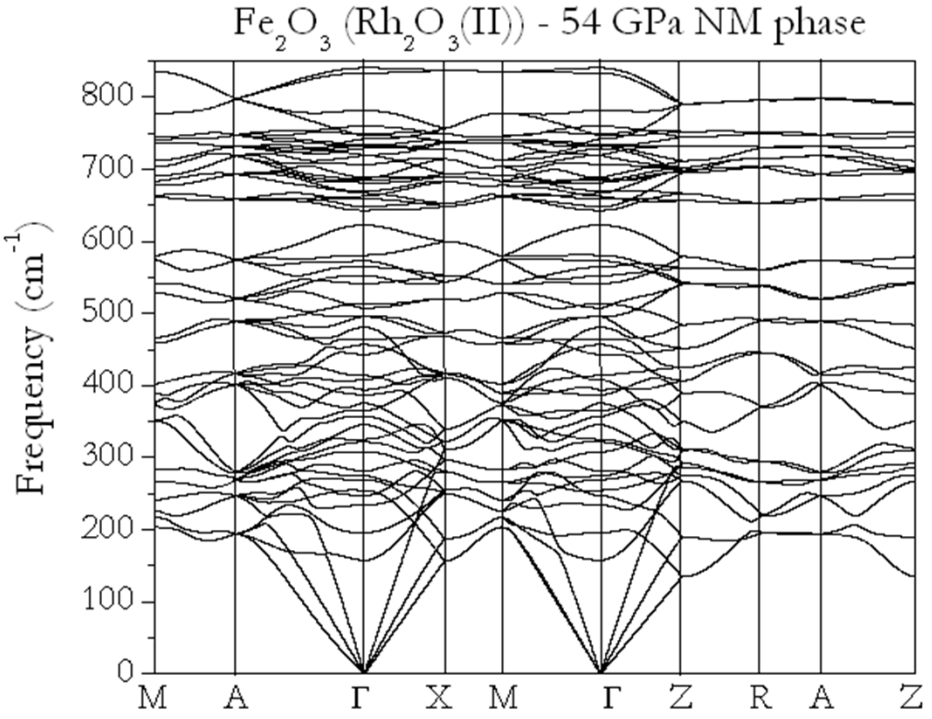
Fe2O3 (Rh2O3(II)) - 54 GPa NM phase
Frequency (cm-1)
800
700
600
500
400
300
200
100
0
M
A
Γ
X
M
Γ
Z
R
A
Z

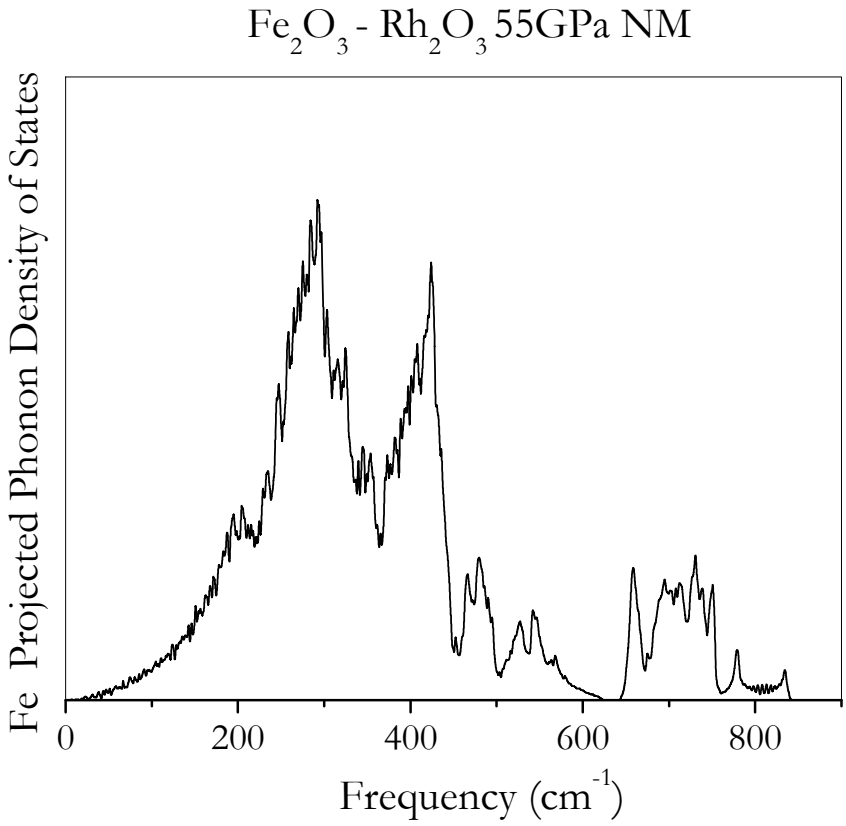
Fe2O3 - Rh2O3 55GPa NM
Fe Projected Phonon Density of States
0
200
400
600
800
Frequency (cm-1)

FIG6

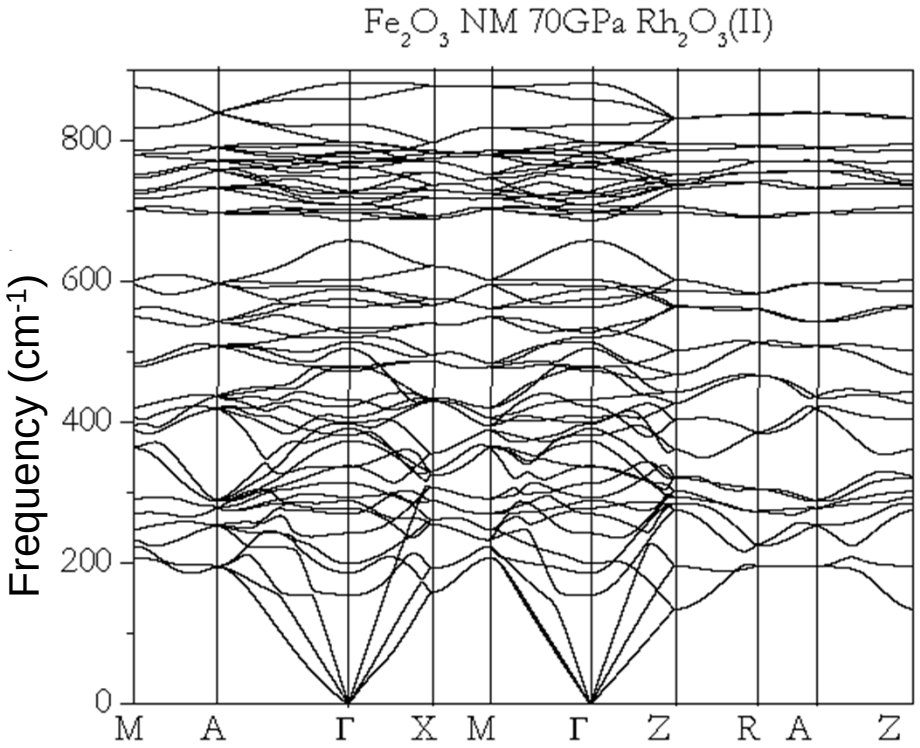
Fe2O3 NM 70GPa Rh2O3(II)
Frequency (cm-1)
800
600
400
200
0
M
A
Γ
X
M
Γ
Z
R
A
Z

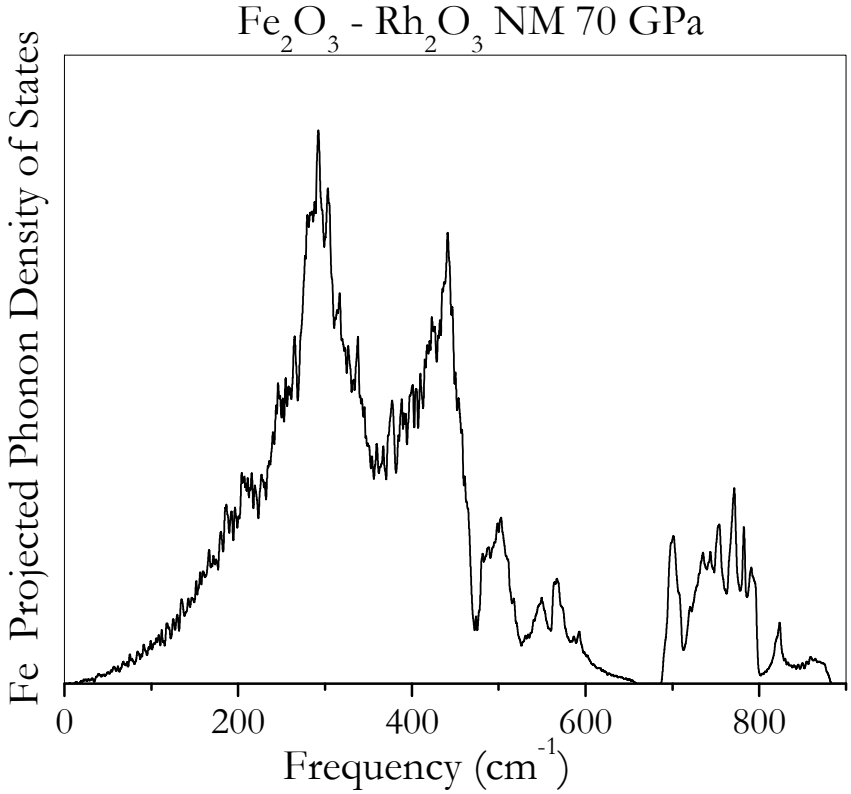
Fe2O3 - Rh2O3 NM 70 GPa
Fe Projected Phonon Density of States
0
200
400
600
800
Frequency (cm-1)

FIG7

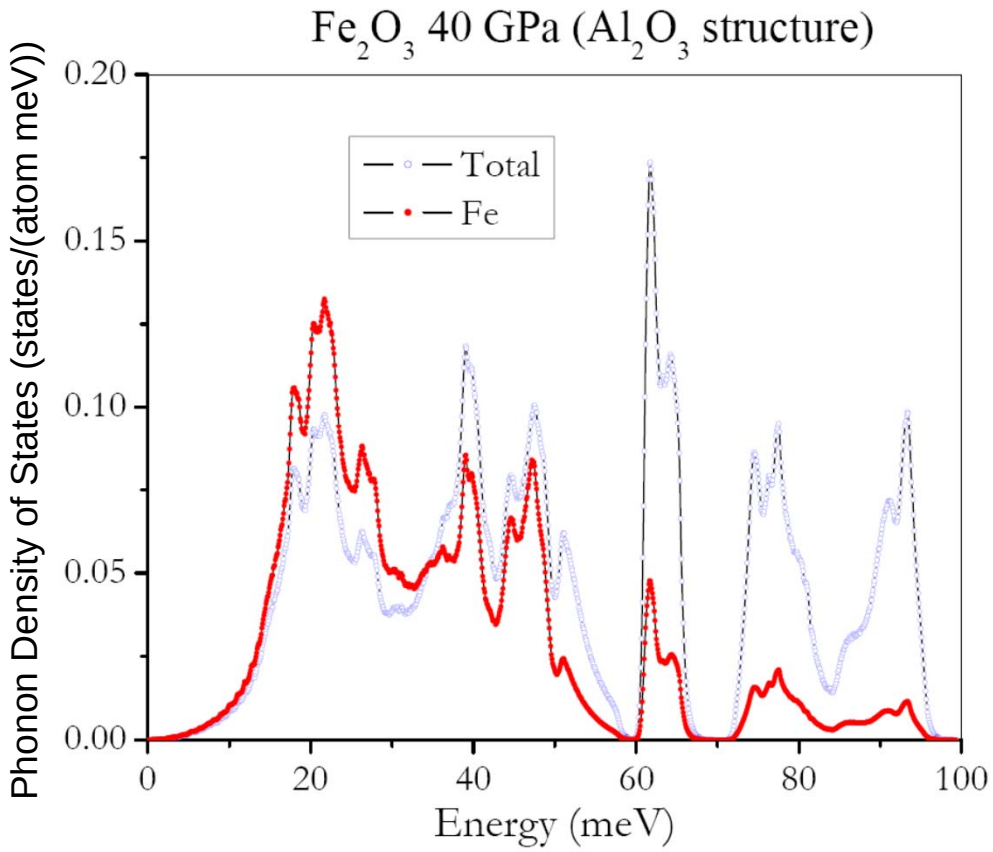
Fe2O3 40 GPa (Al2O3 structure)
Phonon Density of States (states/(atom meV))
Energy (meV)
Total
Fe
0.00
0.05
0.10
0.15
0.20
0
20
40
60
80
100

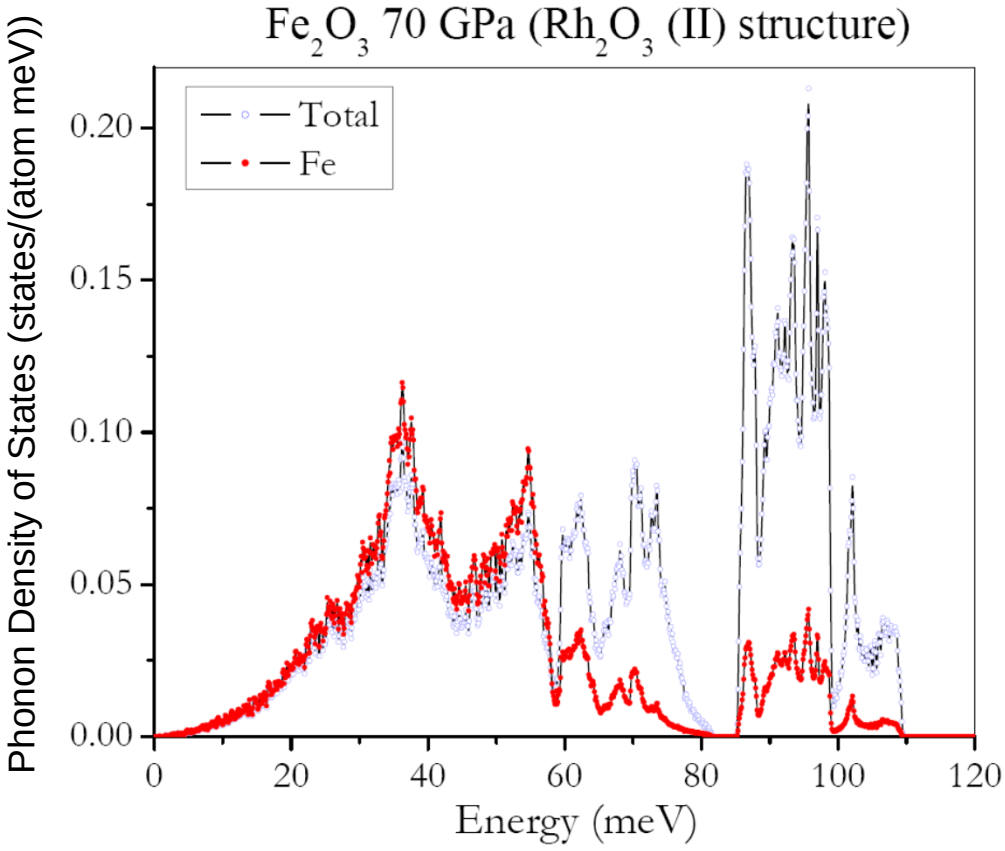
Fe2O3 70 GPa (Rh2O3 (II) structure)
Phonon Density of States (states/(atom meV))
Energy (meV)
Total
Fe
0.00
0.05
0.10
0.15
0.20
0
20
40
60
80
100
120

FIG8